August 25, 2014

Measurement of the Higgs decay width in the diphoton channel

Jonatan Adolfsson[1,2]

[1]Lund University
[2]CERN

Abstract

In this note, a projected measurement of the Higgs decay width (Γ_H) is presented, based on interference in the diphoton channel. Two different hypotheses were tested. Hypothesis A assumes that the $H \to \gamma\gamma$ cross-section is proportional to Γ_H^{-1}, whereas hypothesis B assumes that this cross-section is constant and instead uses the overall change in $m_{\gamma\gamma}$ line shape.

Events were simulated using Sherpa 2.1, and were used to produce test statistics in order to obtain a 95 % confidence limit of Γ_H. The standard model width was tested using Asimov data sets, which were validated using pseudo-experiments for the integrated luminosities of Run 1, Run 2 and HL-LHC. The obtained limits are significantly improved with respect to previous studies, but further validations of the test are required. The expected limits for 300 fb^{-1}are $1.19 \times \Gamma_{HSM}$ for hypothesis A and $24 \times \Gamma_{HSM}$ for hypothesis B.

Contents

1 Introduction 1

1.1 Interference . . . 2

2 Method 2

2.1 Extraction of data . . . 2

2.2 Hypothesis tests . . . 3

3 Hypotheses 3

3.1 k-factors . . . 4

4 Results 4

4.1 Hypothesis A . . . 4

4.2 Hypothesis B . . . 5

5 Discussion 7

6 Conclusions 8

7 Acknowledgements 8

1 Introduction

With the discovery of the Higgs boson during Run 1 of the LHC, the last piece of the Standard Model (SM) was discovered. It is, however, not yet certain whether the discovered Higgs boson is really the SM Higgs. Even if it is the SM Higgs boson, there could be some underlying new physics which affects its properties. Therefore it is important to measure the properties of the Higgs boson. One of the cleanest channels for decay of the Higgs boson is the diphoton channel, and therefore this channel is studied in this project.

One such measurement is to measure the decay width, Γ_H, of the Higgs boson, which defines the width of the diphoton mass resonance ($m_{\gamma\gamma}$)[1] and gives an indirect mesurement on the lifetime of the Higgs boson, τ_H, which is

$$\tau_H = \frac{\hbar}{\Gamma_H}. \tag{1}$$

According to the SM, $\Gamma_H = 4.07$ MeV, which unfortunately is much less than the resolution in the detector, which is about 1.5 GeV (in this project, the previous calculation of the detector resolution, 1.7 GeV, is used). Therefore, an indirect approach is preferred. In this project, two different properties which are affected by the decay width were used in order to put limits on Γ_H: the cross-section in the diphoton channel and the $m_{\gamma\gamma}$line shape.

The cross-section in the diphoton channel, $\sigma_{H\to\gamma\gamma}$ is defined as

$$\sigma_{H\to\gamma\gamma} \equiv \sigma_H \cdot \mathcal{B}(H \to \gamma\gamma) = \frac{\sigma_H \cdot \Gamma_{H\to\gamma\gamma}}{\Gamma_H}, \tag{2}$$

[1]This follows a Breit-Wigner distribution.

where σ_H is the combined cross-section from all channels and $\Gamma_{H\to\gamma\gamma}$ is the decay width in the diphoton channel. Assuming SM $\Gamma_{H\to\gamma\gamma}$ and σ_H,

$$\sigma_{H\to\gamma\gamma} \propto \Gamma_H^{-1}, \tag{3}$$

which means that a lower cross-section in the diphoton channel is expected for greater decay widths.

We can, however, not be sure that $\Gamma_{H\to\gamma\gamma}$ follows the standard model. Another approach is therefore to look at the change in shape of the signal peak when increasing the width.

1.1 Interference

Apart from broadening of the peak, interference between signal ($pp \to H \to \gamma\gamma$) and background ($pp \to \gamma\gamma$) causes a change in line shape when increasing Γ_H. Interference can be understood by expanding the matrix elements after having summed signal and background:

$$|M_s + M_b|^2 = |M_s|^2 + 2 \cdot |M_s \cdot M_b| + |M_b|^2, \tag{4}$$

where M_s and M_b are the matrix elements of signal and background, respectively. In particular, there is interference between $gg \to \gamma\gamma$ (background) and $gg \to H \to \gamma\gamma$ (cf. figure 1).

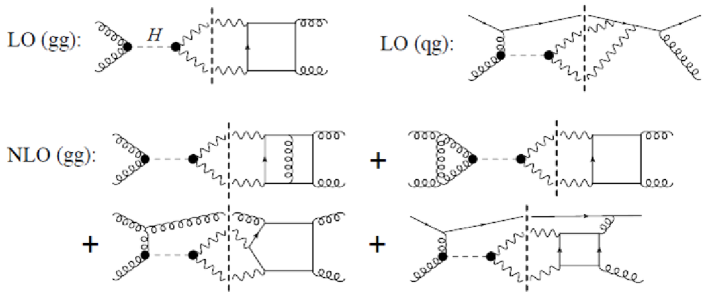

Figure 1: Feynman diagrams showing interference between Higgs production (lefthand side of dashed line) and background (righthand side) in gg-fusion. Source: [1].

2 Method

2.1 Extraction of data

The data samples were obtained using Monte Carlo simulations in Sherpa 2.1, which correctly accounts for interference between signal and background at next-to-leading order (NLO) with respect to the strong interaction. Separate samples were produced for nine different values of Γ_H (1, 10, 50, 100, 200, 400, 600, 800 and 1000 SM widths) by Stefan Hoeche [2], which were complemented by me by adding samples at 0.05 and 0.5 SM widths in order to be able to perform tests also at a smaller width than that of the SM. However, there was an issue with a mismatch between mine and Stefan Hoeche's simulations for interference, which has not yet been resolved. The samples were produced for interference (of $gg \to \gamma\gamma$ with $gg \to H \to \gamma\gamma$) and for signal ($gg \to H \to \gamma\gamma$) for pp collisions at 8 TeV and a Higgs mass of 125 GeV. The samples were either generated inclusively, or separated using a cut at 30 GeV on the Higgs diphoton transversal momentum ($p_T^{\gamma\gamma}$) to increase the sensitivity, since the interference effects are stronger at low $p_T^{\gamma\gamma}$. The resulting line shapes were analysed in a mass window of 100 to 150 GeV. For each width 16 million events were generated.

The line-shape for signal and interference were convoluted with a Gaussian with σ = 1.7 GeV to account for the typical detector resolution at ATLAS. This was done for the line-shapes for $p_T^{\gamma\gamma} < 30$ GeV, $p_T^{\gamma\gamma} > 30$ GeV, and the inclusive events.

In order to add background, a fit (exponential of a polynomial of third order) towards data from Run 1 was produced by omitting a region of ±3 GeV around the Higgs mass peak. Since this data covered a mass window of 105-160 GeV, futher analyses were performed in the window of 105-150 GeV. The signal and background from Sherpa were scaled to 20.3 fb^{-1}in order to be compatible with the background. The entire analysis was later scaled to 100 fb^{-1}, 300 fb^{-1}(Run 2) and 3000 fb^{-1}(HL-LHC).

To obtain a smooth signal and interference for arbitrary width values, an interpolation between the sampling points was carried out. For the signal, a logarithmic interpolation was used, whereas a simple linear interpolation was used for the interference.

2.2 Hypothesis tests

To determine the expected sensitivity, two approaches were chosen: either so-called Asimov data sets or pseudo-experiments were used. Asimov data sets follow the underlying line shape exactly, assigning each data point with the expected statistical uncertainty for a given integrated luminosity, whereas pseudo-experiments are Poisson samplings of the same underlying line shape. The pseudo-experiments were carried out to validate the results from the Asimov data sets. Both types were produced for the inclusive selection or for the separated low and high $p_T^{\gamma\gamma}$categorisation. For each data set a test statistic, $\Delta\chi^2$, was produced, which was on the form

$$\Delta\chi^2 = \chi^2(\hat{\Gamma}) - \chi^2(\Gamma), \tag{5}$$

where

$$\chi^2(\Gamma) = \sum_{i=0}^{n} \frac{(N_i(\Gamma) - N_i^{\text{obs}})^2}{N_i^{\text{obs}}}, \tag{6}$$

where N_i = signal + background + interference for bin i, $\hat{\Gamma}$ is the test value of Γ and N_i^{obs} is the number of observed events in bin i for a given Asimov data set or pseudo-experiment. For the Asimov data sets, $\Gamma = \Gamma_H$ for the underlying line-shape, whereas for pseudo-experiments, Γ is chosen numerically to minimise χ^2 in (6). The test statistics from low and high $p_T^{\gamma\gamma}$regions were merged to obtain a summed statistics.

The test statistics (5) follows asymptotically a χ^2 distribution with one degree of freedom. Thus, the probability for each data set is given by

$$P(\Delta\chi^2) = \int_{\Delta\chi^2}^{\infty} \chi^2(x; 1\,\text{d.o.f.})\,\mathrm{d}x\,. \tag{7}$$

Note that for the Asimov data sets the second term in (5) vanishes. For the pseudo-experiments, the probabilities calculated from (7) were sorted in order to determine the median and corresponding 68% regions around the median. The 95% confidence limit was then calculated by determining the value of Γ_H for which $P(\Gamma_H) = 0.05$, for either the Asimov or the median of the pseudo-experiment.

3 Hypotheses

Two different hypotheses were used in order to obtain limits for the Higgs decay width, from now on called hypothesis A and hypothesis B. All hypotheses assume the SM and are tested against different decay widths.

Hypothesis A assumes that $\Gamma_{H\to\gamma\gamma}$ aggrees with the SM, which - according to section 1 - implies that $\sigma_{H\to\gamma\gamma} \propto \Gamma_H^{-1}$ (cf. figure 2a).

Hypothesis B assumes that there is new physics which causes $\sigma_{H\to\gamma\gamma}$ to be constant under a change in Γ_H. In practice, this means that the signal part of the Sherpa output must be scaled by Γ_H (relative to the SM) and the interference by $\sqrt{\Gamma_H}$. The reason for the latter is that since the background is constant, the interference term in (4) is scaled by a factor of $\sqrt{|M_s|}$ (cf. figure 2b).

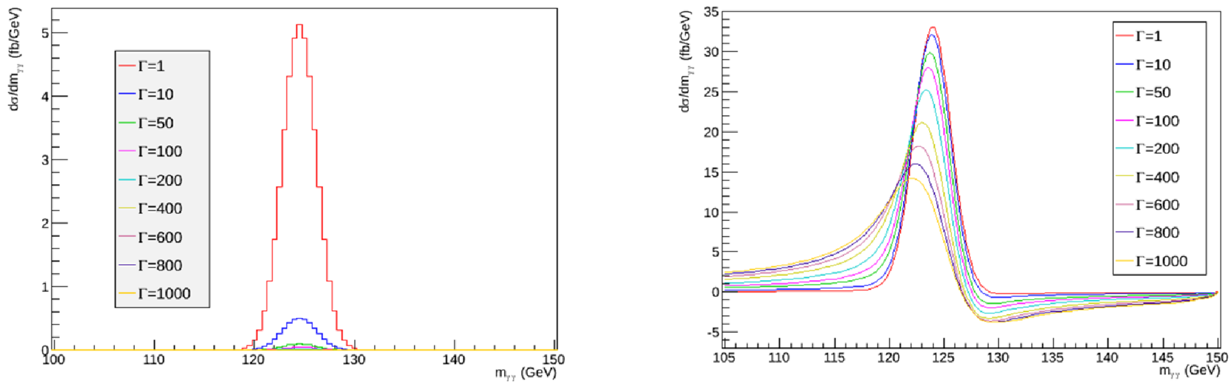

(a) (b)

Figure 2: Dependence on Γ_H for the differential cross-section according to: **(a)** Hypothesis A (note that this plot shows signal only. **(b)** Hypothesis B.

3.1 k-factors

The sherpa NLO cross section needs to be scaled up to correspond to the Higgs cross section working group value [3]. This is done by multiplying signal and interference with a flat factor (called a k-factor). The multiplication of the interference part with k (instead of $\sqrt{k}$) is motivated by the fact that in the soft-collinear limit, QCD radiation cannot resolve the details of the collision process and only see the external legs. Thus the k-factor from signal offers an approximative correction for higher-order effects. This is analogous of what has been done in the width determinations in the $H \to WW$ or $H \to ZZ$ channels. The relevant scale factors used were $k = 1.26$ and $k = 1.76$ ($k = 1$ was tested as a reference), where the latter corresponds to a scaling with the observed coupling strength, $\mu = 1.4$. Note that with this treatment one implicitly assumes that the higher coupling is due to QCD effects, and not to new physics.

The reason for an observed μ of 1.4 might be due to new physics. Therefore, hypothesis A was carried out testing a true $k = 1.76$ scenario with a $k = 1.26$ hypothesis.

4 Results

In this section, results for $k = 1.26$ and $k = 1.76$ for Poisson sampling, splitted into $p_T^{\gamma\gamma}$cuts are shown. More results are given in table 1.

4.1 Hypothesis A

The results for hypothesis A are shown in figure 3 and table 1. Assuming an integrated luminosity of Run 1 and $k = 1.26$, the expected limit on the SM width is $2.8 \times \Gamma_{HSM}$ with 68 % confidence limits at $1.9 \times \Gamma_{HSM}$ and $4.1 \times \Gamma_{HSM}$, respectively. For an integrated luminosity of 300 fb^{-1}and 3000 fb^{-1},

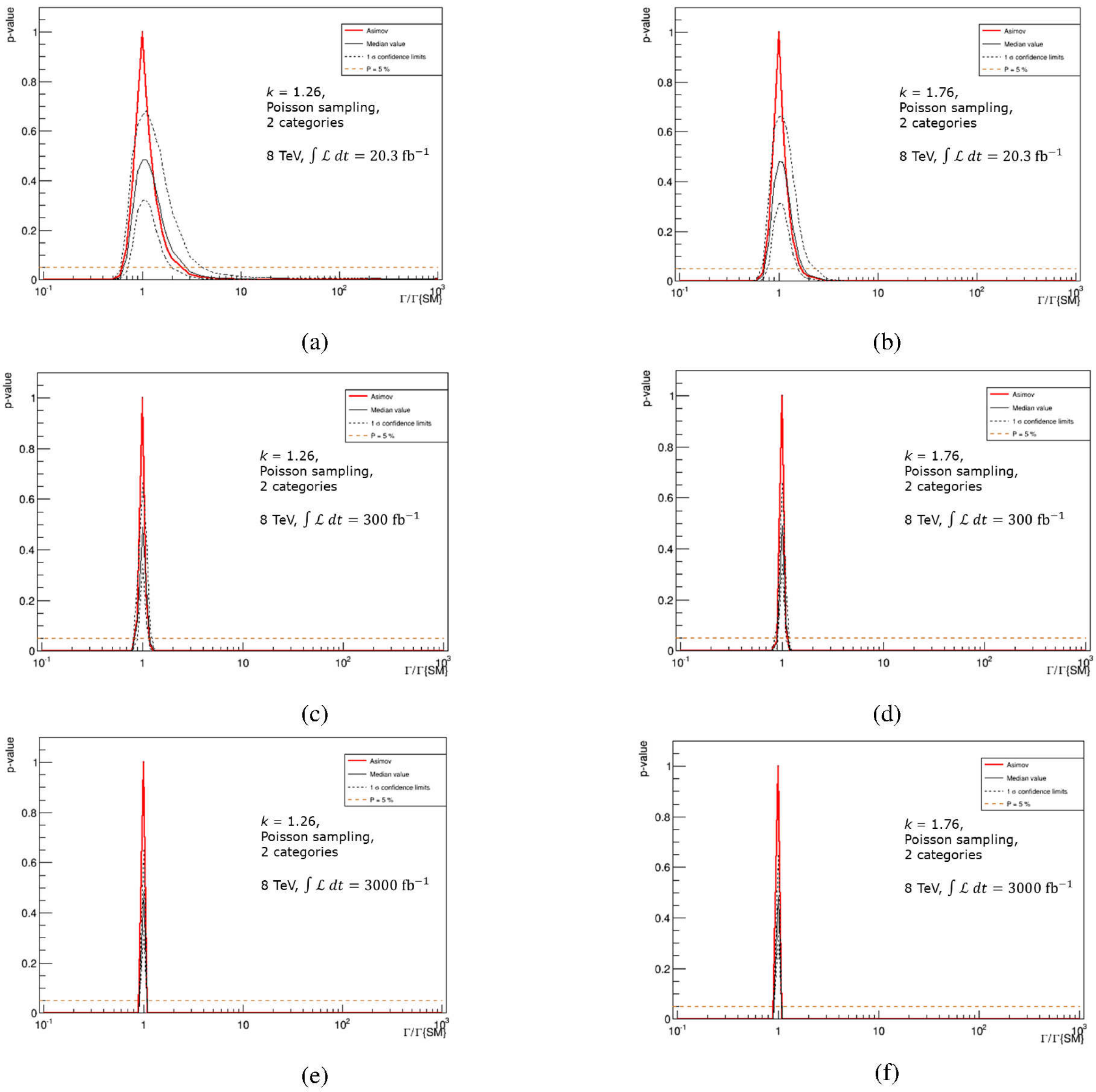

Figure 3: P-values as a function of Γ for hypothesis A. The plots to the left are for $k = 1.26$ and the ones to the right for $k = 1.76$. **(a) and (b)** 20.3 fb^{-1}. **(c) and (d)** 300 fb^{-1}. **(e) and (f)** 3000 fb^{-1}.

one obtains an expected limit of $1.19 \times \Gamma_{HSM}$ and $1.09 \times \Gamma_{HSM}$, respectively, with 68% intervals of $[1.16, 1.25] \times \Gamma_{HSM}$ and $[1.09, 1.09] \times \Gamma_{HSM}$.

The results for the test with $\mu = 1.4$ against $\mu = 1$ for $k = 1.26$ is shown in figure 4 and table 1. Under this scenario, the SM width can be excluded already at 100 fb^{-1}. Assuming this hypothesis, the most likely decay width is $0.7 \times \Gamma_{HSM}$. For high integrated luminosities, the offset of true underlying and test hypothesis causes the probability to be below 5% at all times, hence labelled "n/a" in the table.

4.2 Hypothesis B

The results for hypothesis B are shown in figure 5 and table 1. Assuming an integrated luminosity of Run 1 and $k = 1.26$, the expected limit on the SM width is $340 \times \Gamma_{HSM}$ with 68 % confidence

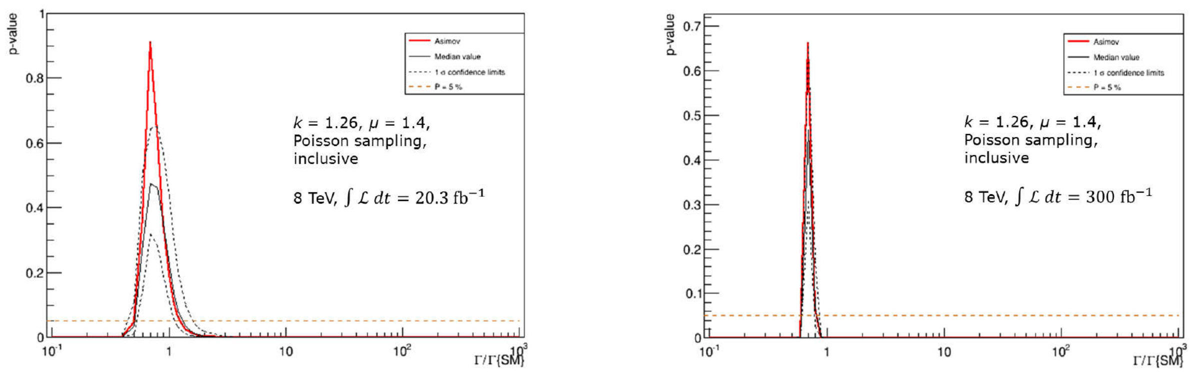

(a) (b)

Figure 4: P-values as a function of Γ for $\mu = 1.4$ tested against $\mu = 1$ for hypothesis A. **(a)** 20.3 fb^{-1}. **(b)** 300 fb^{-1}.

limits at $200 \times \Gamma_{HSM}$ and $590 \times \Gamma_{HSM}$, respectively. For an integrated luminosity of 300 fb^{-1}and 3000 fb^{-1}, one obtains an expected limit of $24 \times \Gamma_{HSM}$ and $5.0 \times \Gamma_{HSM}$, respectively, with 68% intervals of $[17, 36] \times \Gamma_{HSM}$ and $[4.0, 6.6] \times \Gamma_{HSM}$.

Table 1: 95 % confidence limits with 68 % error estimates for all hypotheses

	Hypothesis A			$\mu = 1.4$	Hypothesis B		
20.3 fb^{-1}	$k = 1$	$k = 1.26$	$k = 1.76$	vs. $\mu = 1$	$k = 1$	$k = 1.26$	$k = 1.76$
p_T cuts, Poisson	$4.58^{+10.80}_{-1.77}$	$2.80^{+1.25}_{-0.82}$	$1.79^{+0.61}_{-0.22}$	$1.29^{+0.28}_{-0.16}$	$611.06^{+\infty}_{-262.09}$	$342.23^{+244.67}_{-139.00}$	$163.12^{+95.42}_{-59.47}$
p_T cuts, Gaussian	$4.77^{+58.33}_{-2.01}$	$2.85^{+1.86}_{-0.89}$	$1.83^{+0.75}_{-0.28}$	$1.30^{+0.34}_{-0.19}$	$678.78^{+\infty}_{-291.54}$	$380.03^{+316.21}_{-153.95}$	$184.71^{+104.56}_{-67.70}$
inclusive, Poisson	$4.99^{+23.13}_{-2.16}$	$2.85^{+1.60}_{-0.87}$	$1.83^{+0.64}_{-0.26}$	$1.32^{+0.29}_{-0.19}$	$994.94^{+\infty}_{-446.64}$	$498.49^{+419.18}_{-184.71}$	$230.76^{+148.26}_{-73.40}$
inclusive, Gaussian	$4.86^{+47.51}_{-2.14}$	$2.86^{+1.79}_{-0.92}$	$1.83^{+0.72}_{-0.29}$	$1.32^{+0.33}_{-0.22}$	$915.01^{+\infty}_{-375.76}$	$524.04^{+430.70}_{-207.59}$	$254.90^{+131.09}_{-94.84}$
100 fb^{-1}							
p_T cuts, Poisson	$1.51^{+0.18}_{-0.14}$	$1.37^{+0.11}_{-0.10}$	$1.25^{+0.05}_{-0.07}$	$0.90^{+0.07}_{-0.02}$	$99.16^{+46.80}_{-33.14}$	$65.62^{+27.62}_{-21.28}$	$36.90^{+15.24}_{-12.09}$
p_T cuts, Gaussian	$1.51^{+0.24}_{-0.15}$	$1.38^{+0.14}_{-0.10}$	$1.26^{+0.08}_{-0.07}$	$0.90^{+0.08}_{-0.02}$	$105.93^{+57.90}_{-36.53}$	$70.52^{+35.55}_{-24.10}$	$39.63^{+18.33}_{-13.57}$
inclusive, Poisson	$1.53^{+0.21}_{-0.15}$	$1.38^{+0.12}_{-0.10}$	$1.26^{+0.07}_{-0.07}$	$0.90^{+0.07}_{-0.02}$	$139.36^{+71.73}_{-47.18}$	$89.89^{+45.02}_{-28.01}$	$49.99^{+24.04}_{-14.12}$
inclusive, Gaussian	$1.54^{+0.22}_{-0.17}$	$1.39^{+0.14}_{-0.11}$	$1.27^{+0.08}_{-0.08}$	$0.90^{+0.07}_{-0.03}$	$150.92^{+70.11}_{-51.17}$	$98.22^{+43.83}_{-31.32}$	$54.87^{+23.81}_{-16.94}$
300 fb^{-1}							
p_T cuts, Poisson	$1.25^{+0.06}_{-0.06}$	$1.19^{+0.06}_{-0.03}$	$1.16^{+0.03}_{-0.06}$	$0.85^{+0.03}_{-0.06}$	$35.70^{+16.97}_{-12.97}$	$23.91^{+12.33}_{-7.39}$	$14.47^{+6.21}_{-4.51}$
p_T cuts, Gaussian	$1.25^{+0.08}_{-0.07}$	$1.19^{+0.07}_{-0.03}$	$1.15^{+0.03}_{-0.06}$	$0.85^{+0.03}_{-0.06}$	$39.52^{+18.62}_{-13.39}$	$26.73^{+12.64}_{-8.37}$	$16.09^{+6.50}_{-4.66}$
inclusive, Poisson	$1.26^{+0.06}_{-0.07}$	$1.19^{+0.06}_{-0.03}$	$1.16^{+0.03}_{-0.06}$	$0.83^{+0.05}_{-0.03}$	$51.20^{+21.46}_{-15.86}$	$35.25^{+13.87}_{-11.99}$	$19.94^{+7.72}_{-5.59}$
inclusive, Gaussian	$1.27^{+0.07}_{-0.08}$	$1.20^{+0.07}_{-0.04}$	$1.16^{+0.03}_{-0.06}$	$0.84^{+0.04}_{-0.05}$	$54.98^{+24.43}_{-16.89}$	$37.53^{+17.16}_{-12.08}$	$21.40^{+9.59}_{-6.00}$
3000 fb^{-1}							
p_T cuts, Poisson	$1.09^{+0.00}_{-0.00}$	$1.09^{+0.00}_{-0.00}$	$1.09^{+0.00}_{-0.00}$	n/a	$6.64^{+2.23}_{-1.69}$	$5.03^{+1.64}_{-1.08}$	$3.68^{+0.97}_{-0.73}$
p_T cuts, Gaussian	$1.09^{+0.00}_{-0.01}$	$1.09^{+0.00}_{-0.01}$	$1.09^{+0.00}_{-0.01}$	n/a	$7.18^{+2.45}_{-1.83}$	$5.50^{+1.60}_{-1.31}$	$3.87^{+0.98}_{-0.84}$
inclusive, Poisson	$1.09^{+0.00}_{-0.01}$	$1.09^{+0.00}_{-0.01}$	$1.09^{+0.00}_{-0.01}$	$0.77^{+0.01}_{-0.03}$	$8.60^{+2.92}_{-2.10}$	$6.43^{+1.99}_{-1.48}$	$4.37^{+1.23}_{-0.78}$
inclusive, Gaussian	$1.09^{+0.01}_{-0.01}$	$1.09^{+0.00}_{-0.01}$	$1.09^{+0.00}_{-0.01}$	$0.77^{+0.02}_{-0.04}$	$9.18^{+3.01}_{-2.34}$	$6.76^{+2.13}_{-1.58}$	$4.63^{+1.19}_{-0.92}$

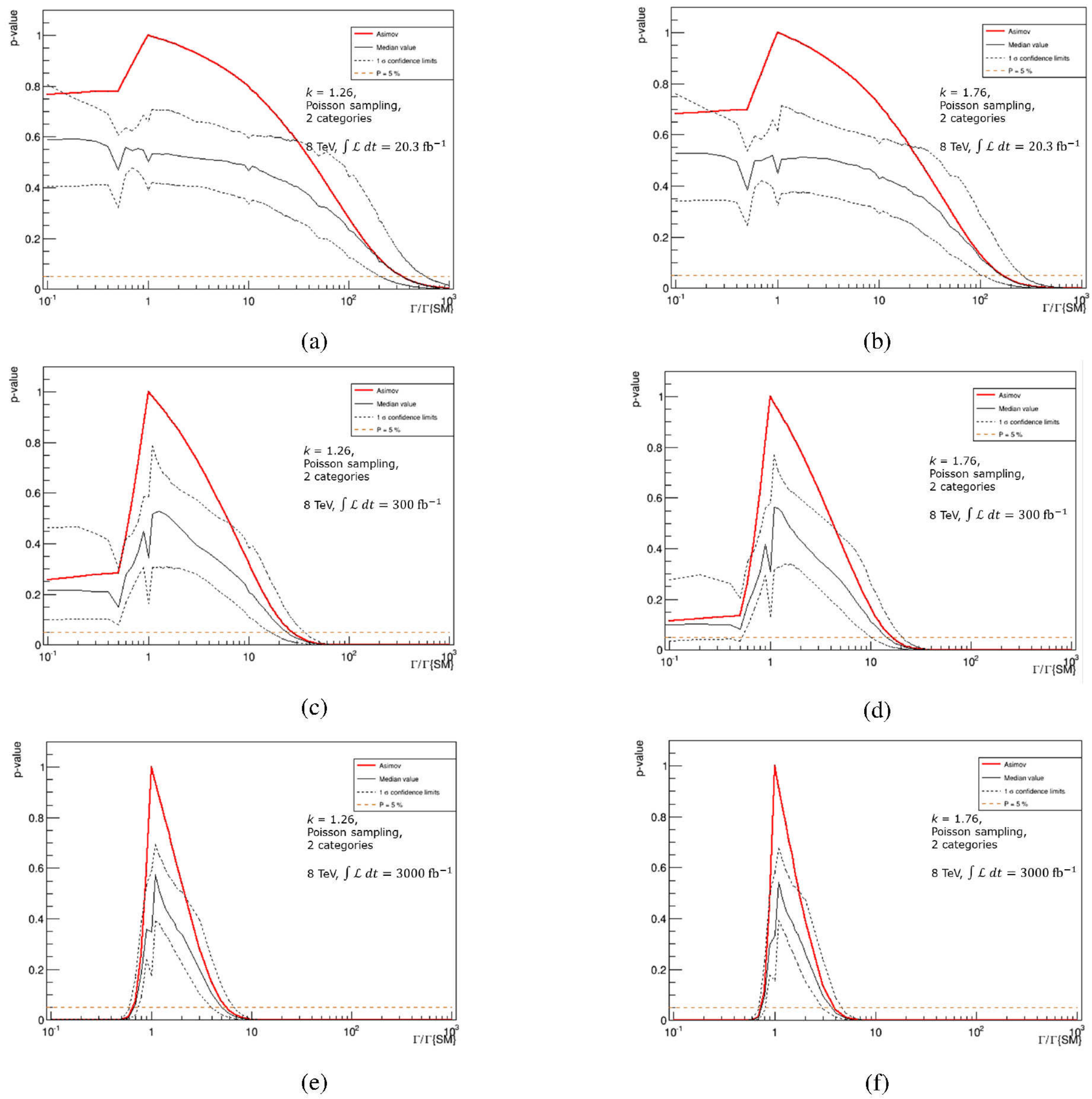

Figure 5: P-values as a function of Γ for hypothesis B. The plots to the left are for $k = 1.26$ and the ones to the right for $k = 1.76$. **(a) and (b)** 20.3 fb^{-1}. **(c) and (d)** 300 fb^{-1}. **(e) and (f)** 3000 fb^{-1}.

5 Discussion

This analysis can be compared to the previous study which looked at the $H \to \gamma\gamma$ decay width in the diphoton channel [4]. The main difference between these studies is that the previous only looked at the apparent mass shift, while this study looks at the overall line shape. This makes this analysis more powerful, and therefore the results are significantly improved. In the previous analysis, the limits on Γ_H are 220 and 40 $\times\Gamma_{HSM}$ (systematic uncertainties neglected) for 300 fb^{-1}and 3000 fb^{-1}, respectively. This means that the limits in this study are improved by a factor 8-10 (for $k = 1.26$). There are, however, some differences in the parameters used, and in the method. The previous study convoluted signal and interference to a crystal ball function ($\sigma = 1.7$ GeV) and used a beam energy of 14 TeV. The latter is important, since this is the energy of Run 2. Due to time constraints, this study was only performed at

8 TeV. For the same amount of data, the sensitivity is expected to improve at 14 TeV: the Higgs cross section increase by a factor of approximately 2.6, while the diphoton background increase by 1.9 [5]. Moreover, the previous study used an analytically calculated line shape as input, while this study used Monte Carlo simulations.

In the previous study, the impact of systematic uncertainties on the limit was evaluated. Doing the same for this study would improve it significantly, and should therefore be subject to future extensions. It is expected that this study is more sensitive to systematics, than the previous one.

Although the results of this study overall seem healthy, they have not yet been fully validated. In particular, the zig-zag pattern and the sudden drop in P-value at lower Γ_H than for the SM need to be investigated further and resolved. The zig-zag pattern is probably due to the interpolation, but it has not been investigated in detail. The drop in P-value is most likely due to the mismatch between mine and Stefan Hoeche's data points. Stefan might have added contribution from quarks to the interference, but this did not resolve the issue completely, when I tried to reproduce it. Therefore, it is likely that the mismatch is due to simulations carried out in different versions of Sherpa. However, at lower P-values, the pseudo-experiments agree well with the results from the Asimov data sets, and therefore the suggested improvements should not affect the results significantly. Instead, one may perform a one-sided test instead.

Moreover, the pseudo-experiments themselves need to be validated. This has been done to a small degree. The χ^2 (see eq. 6) values from the minimisation seem to follow a χ^2 distribution with the appropriate number of degrees of freedom. Moreover, the distrubution of P-values from each pseudo-experiment is uniform between 0 and 1, as expected. However, the errors from the fitted widths do not seem to follow the expected distribution, which needs to be investigated further.

This study has only been carried out for Monte Carlo simulations. In order to actually test the decay width, real data must be used as input. This could be done for the data from Run 1, but since the expected limits for hypothesis B are quite high for Run 1, this should not give so much information. This test should however be carried out for data from Run 2.

The study testing $\mu = 1.4$ against $\mu = 1$ needs to be investigated further. According to Florian Bernlochner, the interference part may not have been taken correctly into account.

6 Conclusions

The method to study the decay width of the Higgs boson in the diphoton channel presented in this report constitute a significant improvement over previously projected measurements. However, the analysis needs to be improved by projecting to higher energy and taking into account systematic uncertainties. Moreover, further validations are required.

7 Acknowledgements

I want to thank my supervisors, Florian Bernlochner and Dag Gillberg for their continuous advice and help with the project. Without them this would not had been possible. I would also like to thank Stefan Hoeche for the data he provided and his help with teaching me Sherpa. My final gratitude goes to the Summer Student Team, who gave me the opportunity to come to CERN to work here as a Summer Student.

References

[1] L. J. Dixon and Y. Li, *Bounding the Higgs Boson Width Through Interferometry*, arXiv:1305.3854 [hep-ph]. Submitted to PRL.

[2] S. Hoeche, *$h \to \gamma\gamma$ analysis*, . http://www.slac.stanford.edu/~shoeche/pub/hint/05/30/.

[3] LHC Higgs Cross Section Working Group, *Handbook of LHC Higgs Cross Sections: 3. Higgs Properties*, arXiv:1307.1347 [hep-ph].

[4] ATLAS Collaboration, *Projections for measurements of Higgs boson cross sections, branching ratios and coupling parameters with the ATLAS detector at a HL-LHC*, ATL-PHYS-PUB-2013-014. http://cds.cern.ch/record/1611186.

[5] M. Quetch-Maitland and A. Pilkington, *$H \to \gamma\gamma$ differential cross section analysis with 100 fb^{-1}*, Higgs Working Group Workshop, Rome. https://indico.cern.ch/event/289241/session/54/contribution/189/material/slides/0.pdf.